Composition-driven spin glass to ferromagnetic transition in the quasicrystal approximant Au-Al-Gd

A. Ishikawa,[1] T. Hiroto,[1] K. Tokiwa,[2] T. Fujii,[3] and R. Tamura[1]

[1]*Department of Materials Science and Technology, Tokyo University of Science, Niijuku, Tokyo 125-8585, Japan*

[2]*Department of Applied Electronics, Tokyo University of Science, Niijuku, Tokyo 125-8585, Japan*

[3]*Cryogenic Research Center, The University of Tokyo, Bunkyo, Tokyo 113-0032, Japan*

(Received 11 March 2015; published 21 January 2016)

We investigated the composition dependence of the magnetic susceptibility of the quasicrystal approximant Au-Al-Gd. A composition-driven ferromagnetic transition is observed in a quasicrystal approximant, which is attributed to the Ruderman-Kittel-Kasuya-Yosida (RKKY) oscillation via a variation in the Fermi wave vector. The ferromagnetic transition is most simply understood as a result of the close matching of the nearest and second-nearest spin distances with the maximum positions of the RKKY potential. The present work provides an idea that allows us to tailor the magnetic order via the electron concentration in quasicrystal approximants as well as in quasicrystals.

DOI: 10.1103/PhysRevB.93.024416

I. INTRODUCTION

Quasicrystal (QC) approximants are periodic crystals that have the same local structure as the corresponding quasicrystals [1]. Since the discovery of the binary quasicrystal $Cd_{5.7}Yb$ [2,3], Tsai-type quasicrystal approximants [4,5], originally identified as being in the close vicinity of the $Cd_{5.7}Yb$ QC, have become a focus of growing interest because of their peculiar structural [6–10], magnetic [11–18], and electronic [19–21] behaviors, which have not been observed in other approximants, such as Mackay- and Bergman-type approximants. For instance, antiferromagnetic (AFM) and ferromagnetic (FM) transitions have been observed in Cd_6R [11–15] and Au-SM-R [16–18] compounds, respectively. Such long-range magnetic order had never before been observed in quasicrystal-related materials [22–27]. Recently, even a superconducting transition has been observed in Au-Ge-Yb [28,29], which is the first example of a superconductor in quasicrystal-related materials.

One major shortcoming of studies on the magnetic properties of Tsai-type approximants may be the lack of a guiding principle for tuning or tailoring the magnetic properties, which has also made it difficult to realize a long-range magnetic order in the corresponding quasicrystals. In this paper, a composition-driven magnetic transition is reported for the Au-Al-Gd quasicrystal approximant. This unusual transition has been observed because of the presence of a widely elongated single-phase domain with a varying Au/Al ratio. The composition-driven magnetic transition is understood to be triggered by a variation in the Fermi wave vector that is induced by the change in the Au/Al ratio. The source of ferromagnetism in this Tsai-type approximant can be attributed to the oscillating Ruderman-Kittel-Kasuya-Yosida (RKKY) interaction.

The crystal structure of Au-Al-Gd resembles that of Au-Al-Tm [30]: Both exhibit the space group $Im\bar{3}$, and both are essentially isostructural with Cd_6Yb, a prototype 1/1 approximant to the icosahedral $Cd_{5.7}Yb$. For this reason, the Au-Al-Gd compound is referred to as an approximant in this paper. As illustrated in Fig. 1, the Au-Al-Gd approximant exhibits bcc packing of so-called Tsai-type icosahedral clusters, which are the same building block found in a number of other compounds such as Cd-R [5] and Ag-In-R [31].

II. EXPERIMENT

Polycrystalline alloys of nominal compositions of Au-Al-Gd were prepared by arc-melting high-purity (>99.9 wt %) Au, Al, and Gd. The alloys were then annealed at 1073 K for 50 h under an Ar atmosphere to obtain an equilibrium phase. The phase purity of the samples was examined by powder x-ray diffraction (XRD) using Cu $K\alpha$ radiation. The temperature and field dependence of the magnetization were measured using a superconducting quantum interference device (SQUID) magnetometer (MPMS, Quantum Design) or a physical property measurement system (PPMS, Quantum Design) equipped with a vibrating sample magnetometer (VSM) in the temperature range between 1.8 and 300 K and at fields of up to 9 T. The temperature dependence of the magnetization was measured during heating under a field of 10 or 100 mT after cooling to the lowest temperature under zero field [zero-field cooling (ZFC)] or a field of 10 mT [field cooling (FC)]. The ac magnetic susceptibility was also measured using MPMS with a field of 0.4 mT and with frequencies of 0.1–1000 Hz. The specific heat measurements were performed using PPMS by the relaxation method between 0.5 and 10 K.

III. RESULTS AND DISCUSSION

A. Composition dependence of the lattice parameter in Au-Al-Gd

Figure 2 shows powder x-ray diffraction patterns of $Au_xAl_{86-x}Gd_{14}$ with various Au concentrations from $x = 49$ to 72. All the peaks can be assigned to a 1/1 Tsai-type quasicrystal approximant with $a = 14.63-14.80$ Å, showing that a single phase is formed in an extraordinarily wide Au/Al range at 1073 K. The intensity distributions of these peaks are very similar to that calculated from the refined structure model of Au-Al-Tm with space group $Im\bar{3}$ shown on the bottom of the figure [30], suggesting that the phase obtained

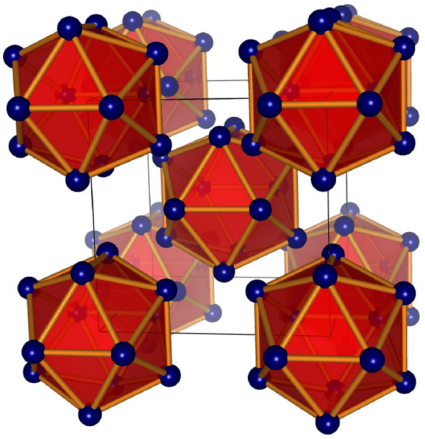

FIG. 1. Crystal structure of the quasicrystal approximant Au-Al-Gd. The Tsai-type icosahedral clusters form a bcc lattice. Only the Gd atoms are shown for clarity. This image was obtained using the VESTA 3 program package [34].

is essentially isostructural to Au-Al-Tm. Figure 3 shows the lattice parameter as a function of the Au concentration in Au-Al-Gd. The lattice parameter increases with increasing Au/Al ratio, which means that Au and Al are mutually replaced over a wide composition range with 14 at.% Gd. Considering that the atomic radii of Au and Al are 1.442 and 1.432 Å [32], respectively, the increase in the lattice parameter with increasing Au/Al ratio can be explained qualitatively by the larger atomic radius of Au as compared to that of Al. We noticed a slight change of the slope at 51 at.% Au and 64 at.% Au in Fig. 3, which may suggest that the replacement between Au and Al atoms occurs not randomly but preferentially owing to the existence of a number of Au/Al mixed sites (seven sites) [30].

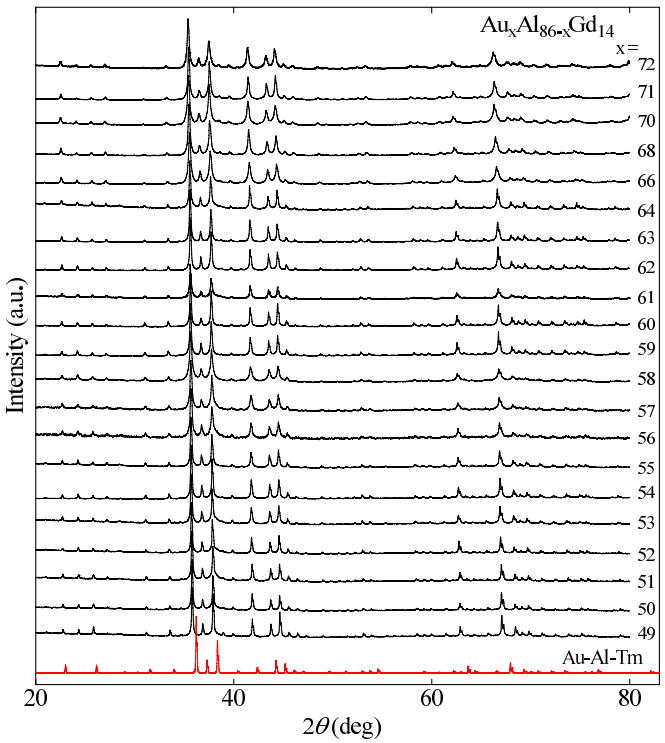

FIG. 2. Powder x-ray diffraction patterns of $Au_xAl_{86-x}Gd_{14}$ with $x = 49-72$. A simulated x-ray diffraction pattern of the isostructural Au-Al-Tm [30] is shown on the bottom for comparison.

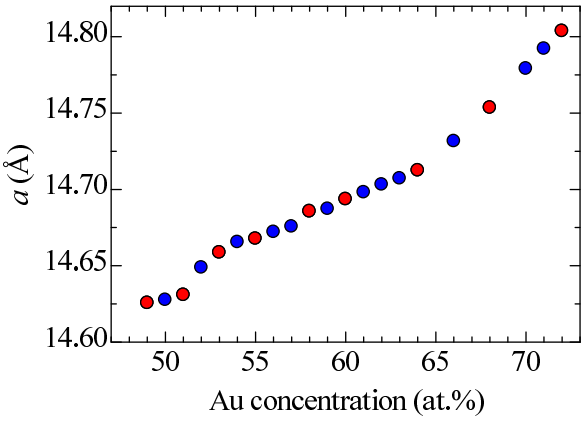

FIG. 3. Lattice parameter as a function of Au concentration in $Au_xAl_{86-x}Gd_{14}$. The solid red circles represent the samples for which magnetic measurement was performed (see Table I).

B. Composition dependence of the magnetic susceptibility of Au-Al-Gd

Figures 4(a) and 4(b) show the temperature dependence of the inverse magnetic susceptibility, $1/\chi$. The inverse magnetic susceptibility values fall perfectly on a straight line in a wide temperature range, well obeying the Curie-Weiss law,

$$\chi(T) = \frac{N_A \mu_{\text{eff}}^2 \mu_B^2}{3k_B(T - \Theta_p)},$$

where k_B, N_A, and μ_B are the Boltzmann constant, Avogadro's number, and the Bohr magneton, respectively. The effective magnetic moment, μ_{eff}, and paramagnetic Curie temperature, Θ_p, values obtained from the fits are listed in Table I. The values of μ_{eff} are in good agreement with the theoretical values for the Gd^{3+} free ion ($7.94\mu_B$), calculated from the Hund's rule ground-state multiplet ($^8S_{7/2}$), which means that the Gd^{3+} spins are well localized on the vertices of the Gd^{3+} icosahedron.

Figure 5 shows the magnetic susceptibility of $Au_{64}Al_{22}Gd_{14}$ below 50 K as a function of temperature. A rapid increase in magnetization, indicative of a ferromagnetic transition, is observed at and above 58 at.% Au, consistent with the positive Θ_p values observed at and above 58 at.% Au. The inset of Fig. 5 shows the magnetization curve at 2 K for $Au_{64}Al_{22}Gd_{14}$. The magnetization rapidly saturates to a value close to the saturation magnetization ($7\mu_B$) estimated from the Hund's rule ground-state multiplet ($^8S_{7/2}$), which confirms the occurrence of a ferromagnetic order below T_c. Thus, all the localized spins on the vertices of the Gd^{3+} icosahedron are collinearly aligned below T_c.

By contrast, there is no magnetic transition below 58 at.% Au, where a bifurcation between the FC and ZFC curves is observed at 2.6 and 3.0 K for $Au_{49}Al_{37}Gd_{14}$ and $Au_{51}Au_{35}Gd_{14}$, respectively [see Figs. 6(a) and 6(c)]. Figures 6(b) and 6(d) show the ac magnetic susceptibility

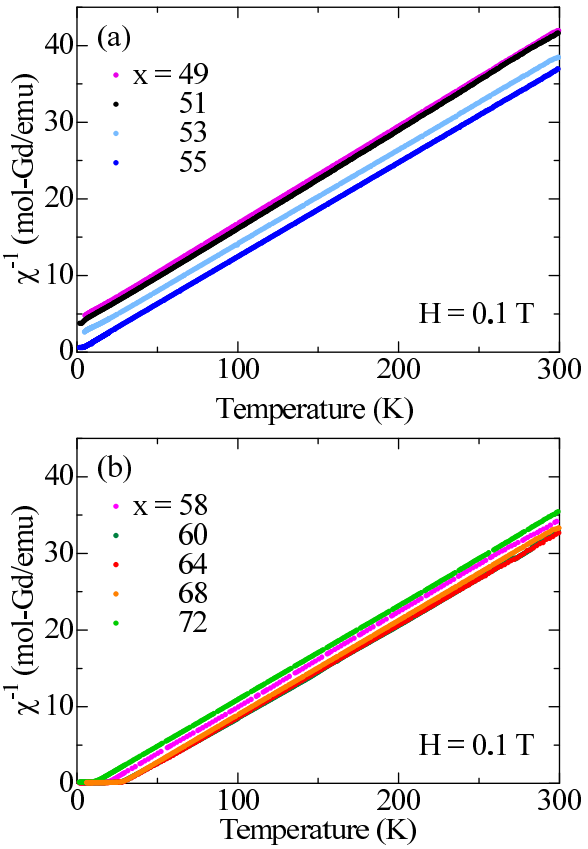

FIG. 4. Temperature dependences of the inverse magnetic susceptibility of $Au_xAl_{86-x}Gd_{14}$. The data are divided into (a) low Au and (b) high Au concentration regions for clarity.

TABLE I. The lattice constant a, paramagnetic Curie temperature Θ_p, Curie temperature T_c, freezing temperature T_f, and effective magnetic moment μ_{eff} of $Au_xAl_{86-x}Gd_{14}$ with $x = 49 - 72$

Au concentration (at.%)	Lattice constant a (Å)	Θ_p (K)	T_f (K)	T_c (K)	μ_{eff} (μ_B)
49	14.6256(2)	−30.4	2.61	–	7.91
50	14.6276(1)	–	–	–	–
51	14.6309(2)	−25.7	3.04	–	7.94
52	14.6489(2)	–	–	–	–
53	14.6587(2)	−14.3	4.00	–	8.08
54	14.6656(2)	–	–	–	–
55	14.6678(2)	−0.35	–	–	8.06
56	14.6722(4)	–	–	–	–
57	14.6757(3)	–	–	–	–
58	14.6857(3)	21.0	–	19.3	7.97
59	14.6873(3)	–	–	–	–
60	14.6936(2)	29.2	–	27.5	7.80
61	14.6982(3)	–	–	–	–
62	14.7033(2)	–	–	–	–
63	14.7073(2)	–	–	–	–
64	14.7125(2)	30.3	–	27.6	8.12
66	14.7316(3)	–	–	–	–
68	14.7536(4)	28.4	–	27.0	8.06
70	14.7792(4)	–	–	–	–
71	14.7923(3)	–	–	–	–
72	14.8039(4)	10.8	–	10.0	8.14

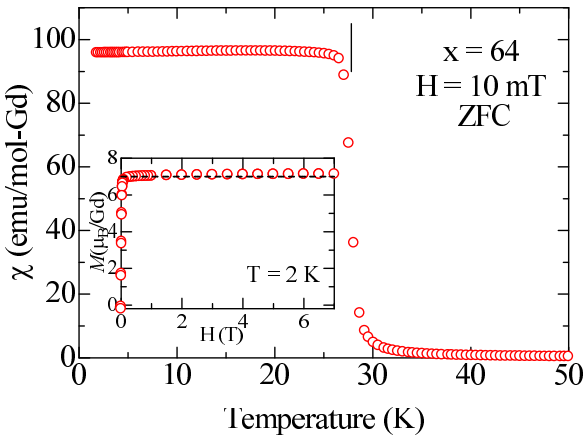

FIG. 5. (a) Temperature dependence of the magnetic susceptibility of $Au_{64}Al_{22}Gd_{14}$. The tick denotes the Curie temperature of 27.6 K.

of $Au_{49}Al_{37}Gd_{14}$ and $Au_{51}Au_{35}Gd_{14}$, respectively, below 4 K with the field frequencies of 0.1–1000 Hz. The cusp temperature is found to increase with increasing the frequency for both samples, which is a characteristic feature of spin-glass freezing. The insets of Figs. 6(a) and 6(c) show the temperature dependence of the specific heat, C_p, for the same samples below 10 K. C_p shows no anomaly but exhibits a broad peak near the cusp temperature, showing the absence of a magnetic transition. The occurrence of spin-glass-like freezing below 58 at.% Au implies the existence of magnetic frustration for each Gd^{3+} spin. One possible origin for the frustration would be an inherent chemical disorder in the Au-Al-Gd compound since chemical disorder between Au and Al is evidenced by the existence of Au/Al mixed sites [30].

C. Origin of the composition-driven ferromagnetic transition in Au-Al-Gd

A salient feature as well as an important finding of the present work is that the paramagnetic Curie temperature, Θ_p, is clearly dependent on the Au/Al ratio, as shown in Fig. 7: Θ_p increases significantly from a large negative value to a large positive value as the Au concentration increases. The obtained Curie temperatures and freezing temperatures are also listed in Table I. A close comparison of the figure and the table shows that the spin-glass behavior is observed only below 55 at.% Au where Θ_p is negative, and the FM order is observed only above 55 at.% Au where Θ_p is positive, indicating that the spin-glass to FM transition is directly related with the sign change of Θ_p.

As for the possible role of structural changes associated with the two features at 51 at.% Au and 64 at.% Au observed in Fig. 3 on the magnetism, we note that Θ_p varies smoothly across the two features and the crossover of the Θ_p value from negative to positive does not coincide with any of the two features (see Figs. 3 and 7). Therefore, it is clear that Θ_p, and hence the magnetic transition, are not affected by possible structural changes associated with the two features.

Figure 7 shows that the net molecular field acting on each Gd^{3+} spin changes from AFM to FM as the Au content increases. We note that the magnetic interaction

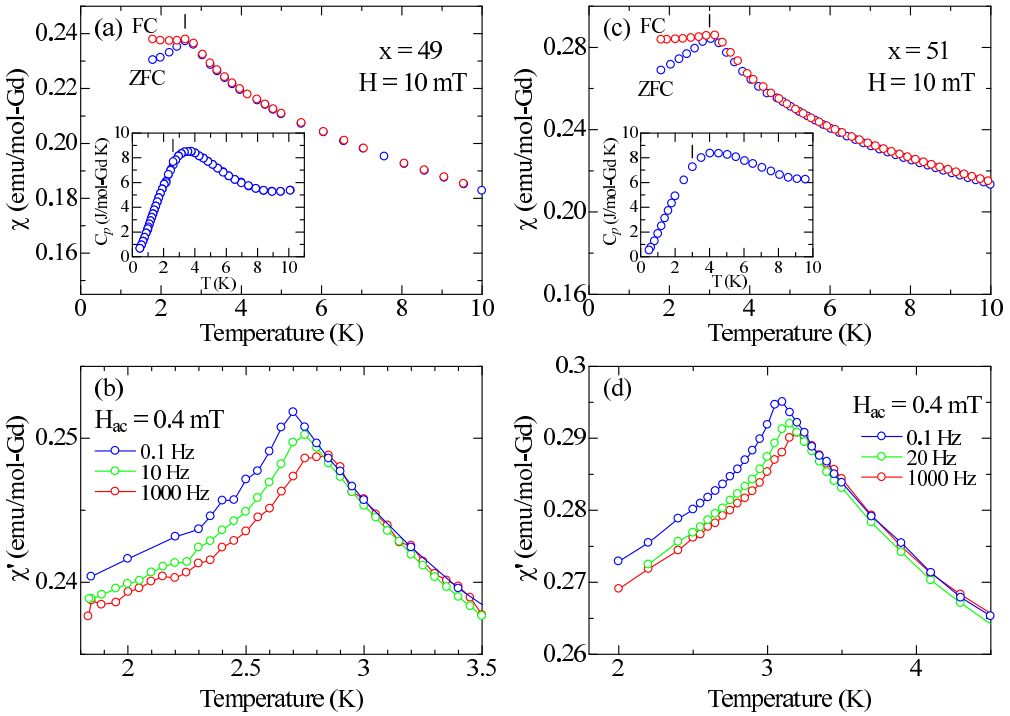

FIG. 6. Temperature dependences of the zero-field-cooled (ZFC) and field-cooled (FC) magnetic susceptibility of (a) $Au_{49}Al_{37}Gd_{14}$ and (c) $Au_{51}Al_{35}Gd_{14}$, respectively. The insets show the temperature dependence of specific heat of the same samples. The ticks denote the freezing temperature of 2.6 and 3.0 K, respectively, obtained from the cusp temperature. Temperature and frequency dependence of the ac magnetic susceptibility for (b) $Au_{49}Al_{37}Gd_{14}$ and (d) $Au_{51}Al_{35}Gd_{14}$, respectively.

between localized Gd^{3+} spins cannot be a direct one; rather, it is mediated through polarization of conduction electrons, which is known as the RKKY interaction [33]. The RKKY interaction, which is expressed by the following equation in the free-electron model, is an oscillating potential with respect to the distance between a pair of localized spins, namely, $\mathbf{S}_1$ and $\mathbf{S}_2$.

$$H_{\mathrm{RKKY}} = -9\pi \left(\frac{N}{V}\right)^2 \frac{{j_0}^2}{\varepsilon_F} f(2k_F R_{21}) \mathbf{S}_1 \cdot \mathbf{S}_2,$$

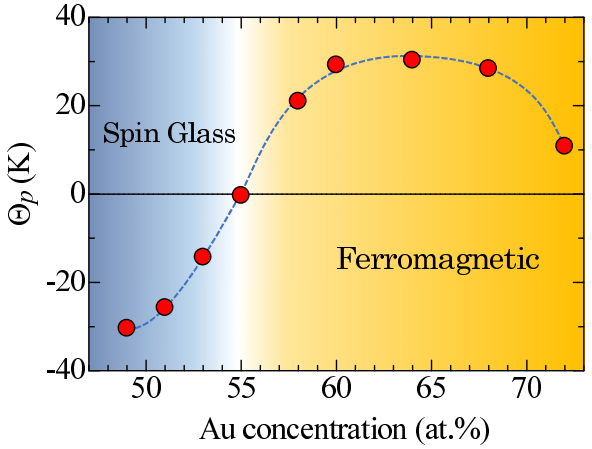

FIG. 7. Paramagnetic Curie temperatures of $Au_xAl_{86-x}Gd_{14}$ as a function of Au concentration.

where N/V, j_0, ε_F, k_F, and R_{21} are the number of electrons in a unit volume, the RKKY coupling strength, the Fermi energy, the Fermi wave vector, and the distance between $\mathbf{S}_1$ and $\mathbf{S}_2$, respectively, and $f(x) = (-x\cos x + \sin x)/x^4$. Thus, FM and AFM interactions occur alternately as R_{21} varies continuously. The observed behavior of Θ_p will now be explained based on the oscillating RKKY interaction. Since the paramagnetic Curie temperature, Θ_p, represents the net strength (including its sign) of the RKKY interaction acting on a single spin from the surrounding spins, the observed sign change in Θ_p in Au-Al-Gd is attributed to the oscillating part $f(2k_F R)$ of the RKKY interaction. Here, we note that a sign change in Θ_p is possible only when $k_F R$ varies with changing Au/Al ratio.

The simplest explanation for both the ferromagnetism and the composition-driven FM transition is as follows. On the basis of the fact that Au is monovalent and both Al and Gd are trivalent, the number of free electrons per unit cell is estimated to be 356 for 49 at.% Au and 303 for 64 at.% Au, where the number of atoms within the unit cell is assumed to be 176 according to the structure model of the essentially isostructural Au-Al-Tm [30]. This gives a Fermi wave vector, k_F, of 1.50×10^{10} m^{-1} for 49 at.% Au and 1.41×10^{10} m^{-1} for 64 at.% Au. Figure 8 plots $f(2k_F R)$ as a function of R for 49 and 64 at.% Au, along with the distribution of Gd^{3+} ions as a function of R up to the second-nearest spin distances. It is seen that k_F plays a more important role in the variation of the RKKY interaction between a pair of spins than the spin distance. For 64 at.% Au, both the nearest and second-nearest spin distances are located near the maximum peak positions of the consecutive ferromagnetic peaks, which well accounts for the observed

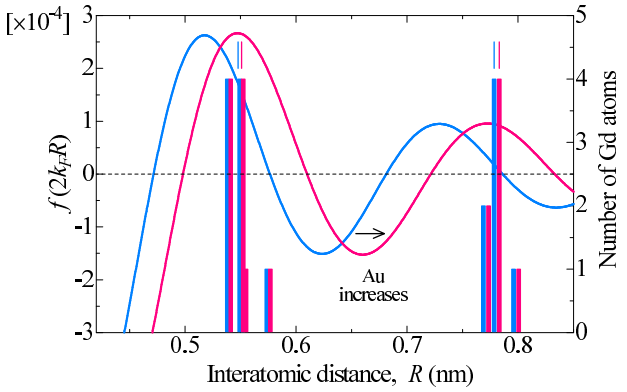

FIG. 8. (Solid curves) Interspin distance dependence of the RKKY interaction, i.e., $f(x) = (-x\cos x + \sin x)/x^4$ where $x = 2k_F R$, for $Au_{49}Al_{37}Gd_{14}$ (blue) and $Au_{64}Al_{22}Gd_{14}$ (red), calculated using the obtained lattice parameters (see Table I) based on the free-electron model. Vertical bars denote the number of Gd spins as a function of R from a single Gd atom for $Au_{49}Al_{37}Gd_{14}$ (blue) and $Au_{64}Al_{22}Gd_{14}$ (red), obtained by using the structural model for the isostructural Au-Al-Tm. The ticks denote the weighted average of the nearest and the second-nearest distances.

large Θ_p as well as the occurrence of the FM order. On the other hand, for 49 at.% Au a substantial deviation of the nearest and second-nearest spin distances from the maximum peak positions is noticed. Thus, in this simplest picture, an increase in k_F by replacing monovalent Au by trivalent Al shifts the RKKY potential curve toward the smaller R region. This gives rise to a reduction of the net FM interaction on each Gd^{3+} spin, resulting in a decrease in Θ_p, which explains the formation of a peak in Θ_p (see Fig. 7). For more quantitative analysis including the magnitude and sign of Θ_p, we need to go beyond the simplest free-electron model.

In this work, the widely elongated single-phase domain along a constant Gd composition of 14 at.% has allowed a substantial variation in the e/a ratio, which has unexpectedly led to observation of a composition-driven FM transition. The present work provides a concept of how to tune or tailor the magnetic order in quasicrystal approximants and related compounds, such as quasicrystals. Further work along these lines is now in progress.

IV. CONCLUSION

The composition dependence of the magnetic susceptibility of the quasicrystal approximant Au-Al-Gd was investigated over a wide range of Au/Al ratio. As a result, a salient composition-driven spin-glass to ferromagnetic transition is observed accompanying a marked change of the paramagnetic Curie temperature. The occurrence of ferromagnetism is most simply understood as the matching of the nearest and second-nearest spin distances with the maximum positions of the oscillating RKKY potential. The present work opens up a route for realizing various magnetic orders in quasicrystal approximants as well as in quasicrystals.

ACKNOWLEDGMENTS

This work was supported by a Grant-in-Aid for Scientific Research (Grant No. 24560808) from Japan Society for the Promotion of Science (JSPS). T.H. acknowledges a Grant-in-Aid for JSPS Fellows (Grant No. 12J07852) from JSPS. Magnetic measurements were in part performed using the facilities of the Institute for Solid State Physics (ISSP), University of Tokyo.

[1] D. Shechtman, I. Blech, D. Gratias, and J. W. Cahn, Phys. Rev. Lett. **53**, 1951 (1984).
[2] A. P. Tsai, J. Q. Guo, E. Abe, H. Takakura, and T. J. Sato, Nature **408**, 537 (2000).
[3] J. Q. Guo, E. Abe, and A. P. Tsai, Phys. Rev. B **62**, R14605 (2000).
[4] A. P. Tsai, Chem. Soc. Rev. **42**, 5352 (2013).
[5] C. P. Gómez and S. Lidin, Phys. Rev. B **68**, 024203 (2003).
[6] R. Tamura, Y. Murao, S. Takeuchi, M. Ichihara, M. Isobe, and Y. Ueda, Jpn. J. Appl. Phys. **41**, L524 (2002).
[7] T. Ishimasa, Y. Kasano, A. Tachibana, S. Kashimoto, and K. Osaka, Philos. Mag. **87**, 2887 (2007).
[8] T. Yamada, R. Tamura, Y. Muro, K. Motoya, M. Isobe, and Y. Ueda, Phys. Rev. B **82**, 134121 (2010).
[9] K. Nishimoto, T. Sato, and R. Tamura, J. Phys.: Condens. Matter **25**, 235403 (2013).
[10] R. Tamura, J. Phys.: Condens. Matter **27**, 085401 (2015).
[11] R. Tamura, Y. Muro, T. Hiroto, K. Nishimoto, and T. Takabatake, Phys. Rev. B **82**, 220201(R) (2010).
[12] M. G. Kim, G. Beutier, A. Kreyssig, T. Hiroto, T. Yamada, J. W. Kim, M. de Boissieu, R. Tamura, and A. I. Goldman, Phys. Rev. B **85**, 134442 (2012).
[13] R. Tamura, Y. Muro, T. Hiroto, H. Yaguchi, G. Beutier, and T. Takabatake, Phys. Rev B **85**, 014203 (2012).
[14] A. Mori, H. Ota, S. Yoshiuchi, K. Iwakawa, Y. Taga, Y. Hirose, T. Takeuchi, E. Yamamoto, Y. Haga, F. Honda, R. Settai, and Y. Ōnuki, J. Phys. Soc. Jpn. **81**, 024720 (2012).
[15] A. Kreyssig, G. Beutier, T. Hiroto, M. G. Kim, G. S. Tucker, M. de Boissieu, R. Tamura, and A. I. Goldman, Philos. Mag. Lett. **93**, 512 (2013).
[16] T. Hiroto, G. H. Gebresenbut, C. P. Gómez, Y. Muro, M. Isobe, Y. Ueda, K. Tokiwa, and R. Tamura, J. Phys.: Condens. Matter **25**, 426004 (2013).
[17] T. Hiroto, K. Tokiwa, and R. Tamura, J. Phys.: Condens. Matter **26**, 216004 (2014).
[18] G. H. Gebresenbut, M. S. Andersson, P. Beran, P. Manuel, P. Nordblad, M. Sahlberg, and C. P. Gómez, J. Phys.: Condens. Matter **26**, 322202 (2014).
[19] T. Watanuki, S. Kashimoto, D. Kawana, T. Yamazaki, A. Machida, Y. Tanaka, and T. J. Sato, Phys. Rev. B **86**, 094201 (2012).
[20] K. Deguchi, S. Matsukawa, N. K. Sato, T. Hattori, K. Ishida, H. Takakura, and T. Ishimasa, Nat. Mater. **11**, 1013 (2012).
[21] S. Jazbec, S. Vrtnik, Z. Jagličic, S. Kashimoto, J. Ivkov, P. Popčevic, A. Smontara, H. J. Kim, J. G. Kim, and J. Dolinšek, J. Alloys Compd. **586**, 343 (2014).
[22] T. J. Sato, Acta Crystallogr. A **61**, 39 (2005).
[23] F. Hippert and J. J. Préjean, Philos. Mag. **88**, 2175 (2008).

[24] S. Ibuka, K. Iida, and T. J. Sato, J. Phys.: Condens. Matter **23**, 056001 (2011).
[25] A. I. Goldman, T. Kong, A. Kreyssig, A. Jesche, M. Ramazanoglu, K. W. Dennis, S. L. Bud'ko, and P. C. Canfield, Nat. Mater. **12**, 714 (2013).
[26] T. Kong, S. L. Bud'ko, A. Jesche, J. McArthur, A. Kreyssig, A. I. Goldman, and P. C. Canfield, Phys. Rev. B **90**, 014424 (2014).
[27] A. I. Goldman, Sci. Technol. Adv. Mater. **15**, 044801 (2014).
[28] K. Deguchi, M. Nakayama, S. Matsukawa, K. Imura, K. Tanaka, T. Ishimasa, and N. K. Sato, J. Phys. Soc. Jpn. **84**, 023705 (2015).
[29] K. Deguchi, M. Nakayama, S. Matsukawa, K. Imura, K. Tanaka, T. Ishimasa, and N. K. Sato, J. Phys. Soc. Jpn. **84**, 015002 (2015).
[30] K. Tanaka, Y. Tanaka, T. Ishimasa, M. Nakayama, S. Matsukawa, K. Deguchi, and N. K. Sato, Acta Phys. Pol. A **126**, 603 (2014).
[31] Y. Morita and A. P. Tsai, Jpn. J. Appl. Phys. **47**, 7975 (2008).
[32] W. B. Pearson, *The Crystal Chemistry and Physics of Metals and Alloys* (Wiley, New York,1972).
[33] K. Yosida, Phys. Rev. **106**, 893 (1957).
[34] K. Momma and F. Izumi, J. Appl. Crystallogr. **44**, 1272 (2011).